

Electronic Supplementary Information

Thermal C-O coupling reactions of Ta methylene clusters $[\text{Ta}_n\text{CH}_2]^+$ ($n = 1,4$) with O_2

T. Masubuchi,^{a,†} J. F. Eckhard,^{a,†} G. Goddard,^a M. Tschurl,^{a*} and U. Heiz^a

^a Lehrstuhl für Physikalische Chemie, Chemistry Department & Catalysis Research Center, Technische Universität München, Lichtenbergstr. 4, 85748 Garching, Germany

* Corresponding author's e-mail: tschurl@tum.de

† Authors contributed equally to the work.

1. Assignment of species (reactions in He, CH₄ and ¹⁸O₂)

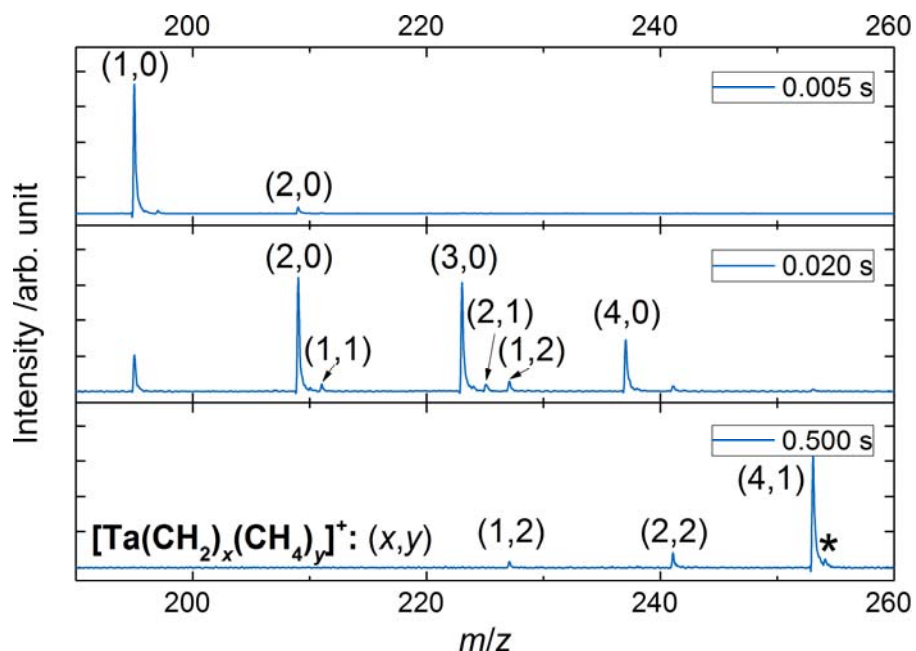


Fig. S1 Time-of-flight mass spectra of $[\text{TaCH}_2]^+$ exposed to CH_4 , depicting the consecutive reaction toward $[\text{Ta}(\text{CH}_2)_2]^+$, $[\text{Ta}(\text{CH}_2)_3]^+$, $[\text{Ta}(\text{CH}_2)_4]^+$ and $[\text{Ta}(\text{CH}_2)_4(\text{CH}_4)]^+$ as well as $[\text{Ta}(\text{CH}_2)(\text{CH}_4)]^+$, $[\text{Ta}(\text{CH}_2)(\text{CH}_4)_2]^+$, $[\text{Ta}(\text{CH}_2)_2(\text{CH}_4)]^+$ and $[\text{Ta}(\text{CH}_2)_2(\text{CH}_4)_2]^+$ as minor species. The asterisk (*) marks a $[\text{Ta}(\text{CH}_2)_4(\text{CH}_4)]^+$ species shifted by a single mass unit as it contains a naturally occurring ¹³C isotope. The same products are observed, when Ta⁺ is exposed to methane.¹⁻³

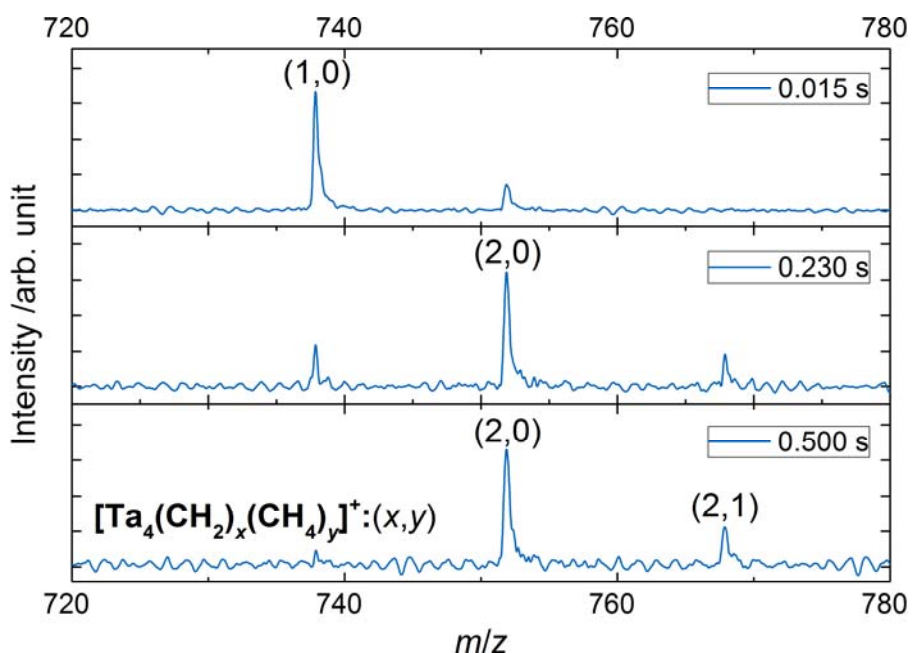


Fig. S2 Time-of-flight mass spectra of $[\text{Ta}_4\text{CH}_2]^+$ exposed to CH_4 , which generates $[\text{Ta}_4(\text{CH}_2)_2]^+$ and $[\text{Ta}_4(\text{CH}_2)_2(\text{CH}_4)]^+$ as seen in the reaction of the bare cluster with methane.⁴

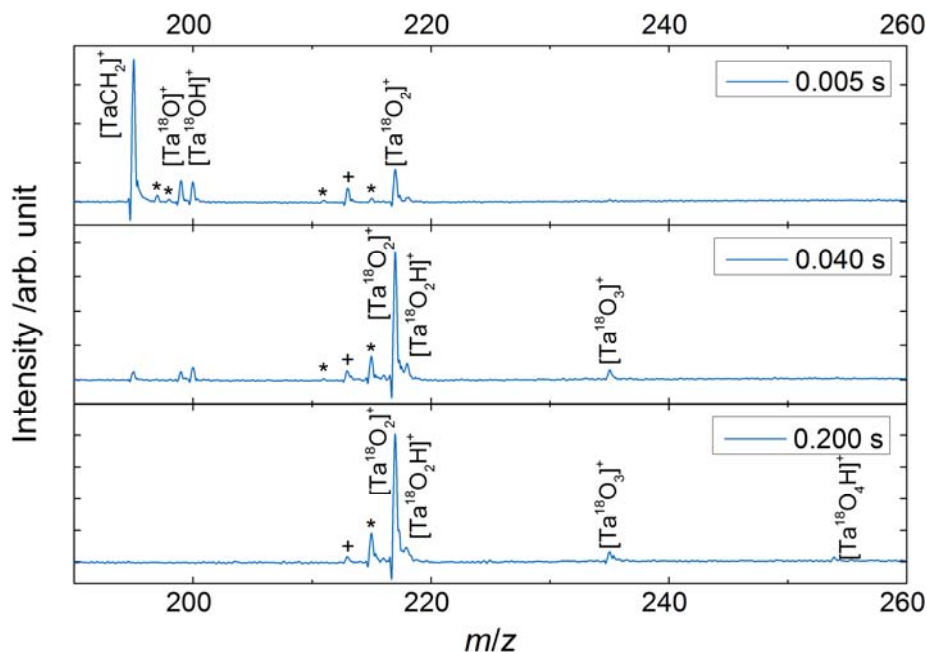


Fig. S3 Time-of-flight mass spectra of $[\text{TaCH}_2]^+$ exposed to $2.8 \cdot 10^{-5}$ Pa $^{18}\text{O}_2$ at 300 K for reaction times of 5, 40 and 200 ms. Products analogous to the ones formed in the reaction with $^{16}\text{O}_2$ are observed. Additionally, $^{16}\text{O}_2$ and $^{16}\text{O}^{18}\text{O}$, impurities in the $^{18}\text{O}_2$ gas cylinder, generate minority species marked by asterisks ($[\text{Ta}^{16}\text{O}]^+$, $[\text{Ta}^{16}\text{OH}]^+$, $[\text{Ta}^{16}\text{OCH}_2]^+$ and $[\text{Ta}^{16}\text{O}^{18}\text{O}]^+$). The peak denoted by a plus sign corresponds to an overlap of $[\text{Ta}^{18}\text{OCH}_2]^+$ and $[\text{Ta}^{16}\text{O}_2]^+$.

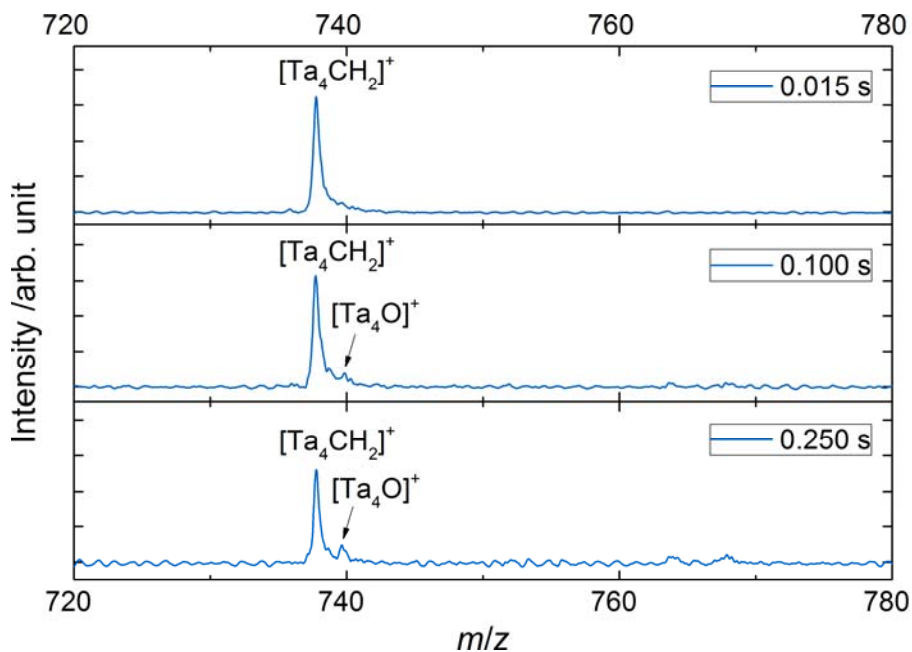


Fig. S4 Time-of-flight mass spectra of $[\text{Ta}_4\text{CH}_2]^+$ stored in helium buffer gas at 300 K, illustrating a reaction with background water that generates a small amount of $[\text{Ta}_4\text{O}]^+$.

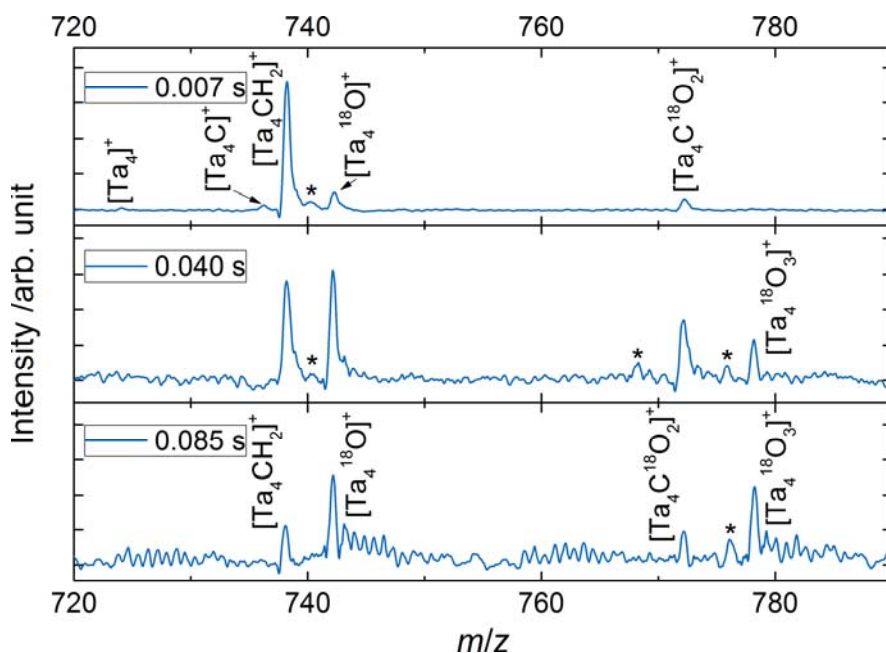


Fig. S5 High-mass range excerpts of time-of-flight mass spectra illustrating the reaction of $[\text{Ta}_4\text{CH}_2]^+$ with $1.8 \cdot 10^{-5}$ Pa $^{18}\text{O}_2$ at 300 K for reaction times of 7, 40 and 85 ms. The oxidation reactions produce species analogous to the ones observed in the reactions with $^{16}\text{O}_2$, i.e. the monoxide, trioxide and carbon-dioxide of the tantalum tetramer cluster cation. In addition, the contaminants in the gas bottle, $^{16}\text{O}^{18}\text{O}$ and $^{16}\text{O}_2$, cause the formation of three side products, $[\text{Ta}_4^{16}\text{O}]^+$, $[\text{Ta}_4\text{C}^{16}\text{O}_2]^+$ and $[\text{Ta}_4^{16}\text{O}^{18}\text{O}_2]^+$, which are respectively marked by asterisks (*).

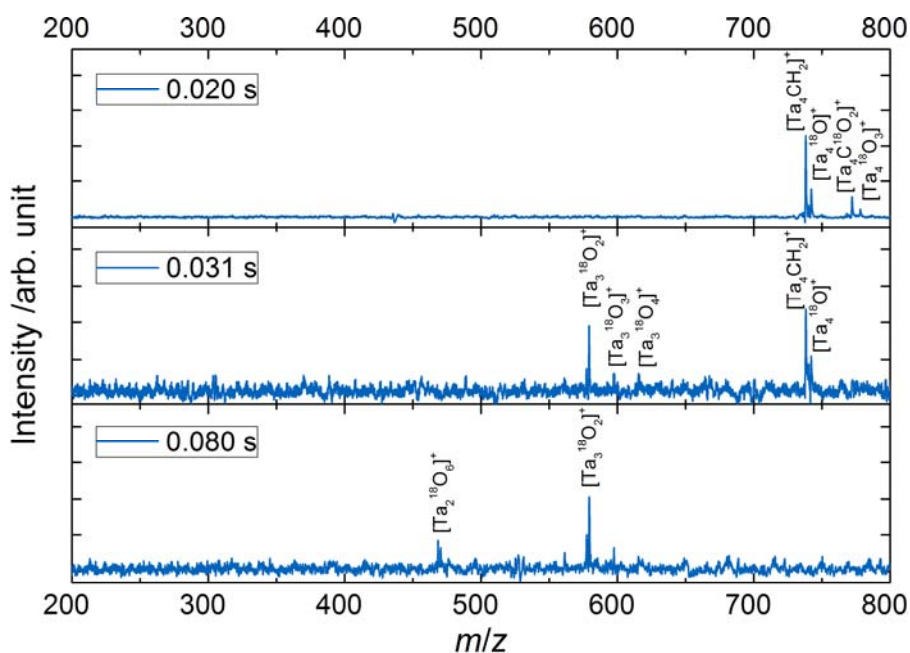


Fig. S6 Time-of-flight mass spectra of $[\text{Ta}_4\text{CH}_2]^+$ exposed to $1.8 \cdot 10^{-5}$ Pa $^{18}\text{O}_2$, illustrating an initial oxidative release of carbon followed by consecutive oxidative degradation reactions of the clusters. Note that, in comparison to the reaction with $^{16}\text{O}_2$, the lower overall signal intensity and poorer storage efficiency prohibit the observation of the full degradation process.

2 Errors and referencing of rate coefficients

Due to differential pumping of the RET from the axial openings and injection of the buffer gas *via* a channel in the center of the trap, an unknown pressure gradient results throughout the trap. Therefore, the locally measured pressure may deviate from the mean value in the RET and be the largest source of errors. Its uncertainty is estimated by others with a similar setup to be 50%⁵ and will be directly reflected in the absolute values for bi- and termolecular rate constants. To remedy this source of error, the obtained rate coefficient for $[\text{TaCH}_2]^+$ formation being $k^{(2)} = 1.15 \cdot 10^{-9} \text{ cm}^3/\text{s}$ is compared to a literature reference² ($k^{(2)} = 3.8 \cdot 10^{-10} \text{ cm}^3/\text{s}$). The corresponding ratio of about three is used as a correction factor for all experimentally determined rate coefficients. Note that the systematic error caused by the absolute pressure and the subsequent correction for it have no impact on the relative error and, thus, the branching ratios. In addition, one has to account for thermal transpiration when the ion trap (and buffer gas) temperature T_a differs from the baratron temperature T_m .^{6, 7} Equation S1 expresses the required correction of the measured pressure P_m to obtain the actual pressure P_a .

$$P_a = P_m \sqrt{T_a/T_m} \quad (\text{S1})$$

As the buffer and reactant gas ensembles obey a Maxwell-Boltzmann energy distribution, multi-collision conditions promote reactions associated with endothermic barriers and products.⁷

3 Kinetic model, rate coefficients and theoretical collision rates

Several kinetic models are evaluated and the simplest one, which represents the experimentally obtained findings the best, is assumed to be the correct one. In this regard it should be noted that a reaction model including the subsequent oxidation of $[\text{Ta}_4\text{CH}_2]^+$ via $[\text{Ta}_4\text{C}]^+$ to $[\text{Ta}_4\text{CO}_2]^+$ is also able to replicate the general experimental findings in Figure 2. However, the tantalum tetramer carbide barely exceeds the noise level and its oxidation reaction would have to proceed with a reaction efficiency of ten times the collision rate predicted by the SCC model (see below). Thus, this alternative reaction model seems very unlikely and is therefore discarded in the analysis of the reaction pathways and rate coefficients.

4 Comparison of reactions of bare tantalum species and corresponding carbenes

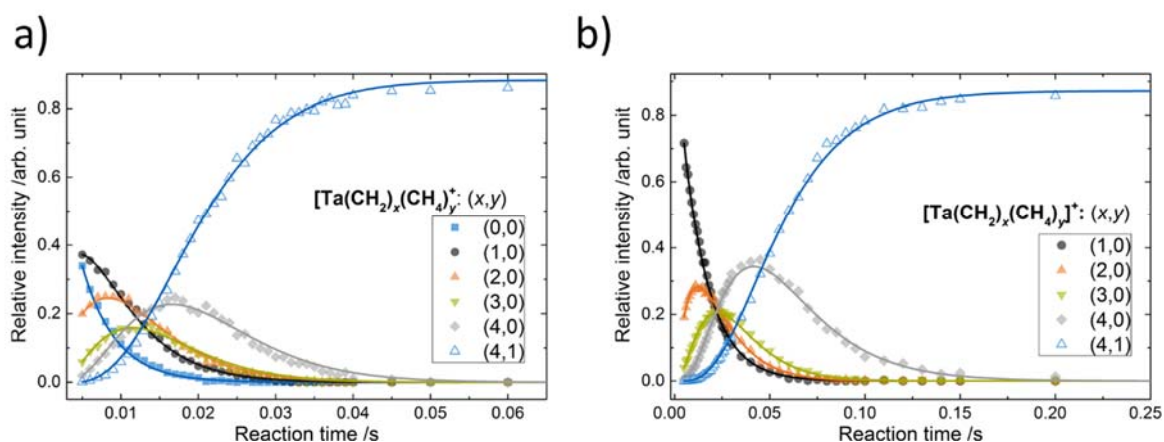


Fig. S7 Comparison of reaction kinetics for the consecutive dehydrogenation of methane by the bare tantalum cation (a) and by the tantalum carbene cation (b). Note that the different time scale is a result of different partial methane pressures ($8.6 \cdot 10^{-2}$ Pa for the bare atomic cation (a) and $2.5 \cdot 10^{-2}$ Pa for $[\text{TaCH}_2]^+$ (b), corresponding to a factor of 3.4). The values for rate coefficients are given in Table S1.

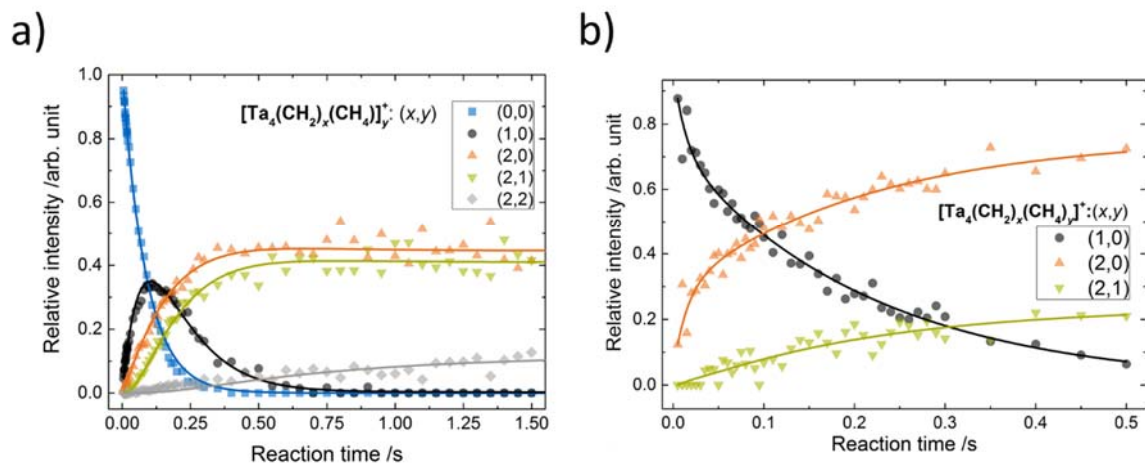


Fig. S8 Comparison of kinetics for the consecutive reactions with methane of the bare tantalum tetramer cation (a) and those of the corresponding carbene (b). Partial pressures are given $8.6 \cdot 10^{-2}$ Pa for the bare tetramer (a) and $2.5 \cdot 10^{-2}$ Pa for $[\text{Ta}_4\text{CH}_2]^+$ (b). The values for rate coefficients are given in Table S1.

Table. S1 Comparison of bimolecular rate coefficients $k^{(2)}$ in units of $10^{-11} \text{ cm}^3\text{s}^{-1}$ in the consecutive reaction of tantalum species toward methane. The reactants exhibit very similar rate coefficients, regardless of their origin of formation (i.e. whether $[\text{Ta}_{1,4}\text{CH}_2]^+$ is generated in the ion trap or in the cluster source).

Species initially entering ion trap	Ta^+	$[\text{TaCH}_2]^+$
Reaction	$k^{(2)}$ [a]	$k^{(2)}$ [a]
$[\text{Ta}(\text{CH}_2)]^+ + \text{CH}_4 \rightarrow [\text{Ta}(\text{CH}_2)_2]^+ + \text{H}_2$	35.20±7.11	38.65±7.80
$[\text{Ta}(\text{CH}_2)_2]^+ + \text{CH}_4 \rightarrow [\text{Ta}(\text{CH}_2)_3]^+ + \text{H}_2$	40.54 ± 8.19	53.44±10.79
$[\text{Ta}(\text{CH}_2)_3]^+ + \text{CH}_4 \rightarrow [\text{Ta}(\text{CH}_2)_4]^+ + \text{H}_2$	55.38±11.20	57.49±11.61
$[\text{Ta}(\text{CH}_2)_4]^+ + \text{CH}_4 \rightarrow [\text{Ta}(\text{CH}_2)_4(\text{CH}_4)]^+$	31.09±6.28	20.74±4.19

Species initially entering ion trap	Ta_4^+	$[\text{Ta}_4\text{CH}_2]^+$
Reaction	$k^{(2)}$ [a]	$k^{(2)}$ [a]
$[\text{Ta}_4(\text{CH}_2)]^+ + \text{CH}_4 \rightarrow [\text{Ta}_4(\text{CH}_2)_2]^+ + \text{H}_2$	0.06 ± 0.01	0.05 ± 0.01
$[\text{Ta}_4(\text{CH}_2)_2]^+ + \text{CH}_4 \rightarrow [\text{Ta}_4(\text{CH}_2)_2(\text{CH}_4)]^+$	0.05 ± 0.01	0.02 ± 0.02

[a] Rate coefficients referenced to $[\text{TaCH}_2]^+$ formation determined by Shayesteh et al.² Uncertainties do not take deviations of absolute pressure into account.

References

1. L. G. Parke, C. S. Hinton and P. B. Armentrout, *J Phys Chem C*, 2007, **111**, 17773-17787.
2. A. Shayesteh, V. V. Lavrov, G. K. Koyanagi and D. K. Bohme, *J Phys Chem A*, 2009, **113**, 5602-5611.
3. V. J. F. Lapoutre, B. Redlich, A. F. G. van der Meer, J. Oomens, J. M. Bakker, A. Sweeney, A. Mookherjee and P. B. Armentrout, *J Phys Chem A*, 2013, **117**, 4115-4126.
4. J. F. Eckhard, T. Masubuchi, M. Tschurl, R. N. Barnett, U. Landman and U. Heiz, *J Phys Chem C*, 2018, **122**, 25628-25637.
5. M. Neumaier, F. Weigend, O. Hampe and M. M. Kappes, *The Journal of Chemical Physics*, 2005, **122**, 104702.
6. R. C. Bell, K. A. Zemski, D. R. Justes and A. W. Castleman, *J Chem Phys*, 2001, **114**, 798-811.
7. T. M. Bernhardt, *Int J Mass Spectrom*, 2005, **243**, 1-29.